CHAPTER 291

SEDIMENT TRANSPORT IN SWASH ZONE UNDER OBLIQUELY INCIDENT WAVES

Toshiyuki Asano[1]

ABSTRACT

Time dependent calculations on two-dimensional sediment transport are carried out. The swash wave front is treated as a moving boundary which can reproduce non-vanishing sediment transport rate even for landward region of the still water shoreline. Meanwhile, experimental investigations on this subject are conducted by florescent sand tracer method. By comparing the present and existing experimental results with the numerical ones, the sediment transport mechanism in the swash zone is discussed.

1. INTRODUCTION

Recently, swash zone has received much attention because the sediment process in this zone provides an important boundary condition for the entire beach evolution. And also, recent studies have reported that the alongshore sand transport takes bimodal distribution with maxima at the swash zone as well as near the breaking point(White-Inman (1986), Bodge-Dean (1987)). Under obliquely incident waves, sediment near shoreline moves in a zig-zag way which results in the inherent alongshore transport in the swash zone. Intensive turbulence generated in uprush and backwash waves causes a large volume of sediment in suspension. However, these mechanisms have not been sufficiently understood.

The author proposed a horizontally two-dimensional shallow water wave model for predicting the free surface elevation and fluid velocities in the swash and surf zone under obliquely incident waves (Asano, 1994). The

---

[1] Associate Professor, Dept. of Ocean Civil Engrg., Kagoshima Univ., 1-21-40, Korimoto, Kagoshima, 890, JAPAN

sediment movement in swash zone should be described in a time dependent way because the bed is immersed and dried alternatively corresponding to run-up and run-down motion. The objective of this work is to improve the understanding of sediment transport in the swash zone by numerical analysis as well as experimental investigations focusing on the alongshore transport rate.

2. NUMERICAL ANALYSIS

(a) Two dimensional velocity fields in swash zone

The author has presented the numerical model for the two-dimensional velocity field in a swash zone (Asano, 1994). The outline of the calculations is as follows:

Two dimensional coordinate system is considered where x- and y- axis is chosen to be in the normal and the parallel direction to the shoreline, respectively. The z-axis is taken positive upward with z=0 at the still water shoreline. The beach slope S is herein restricted to be uniform and its contour is straight and parallel to the shoreline. The incident monochromatic waves with straight parallel crests are assumed to arrive at the seaward boundary with an angle θ_B.

The basic equations are two-dimensional shallow water equations with a moving boundary at the front of wave runup. Ryrie's(1983) method is applied in order to obtain simplified equations. That is, the wave crest is straight parallel and bottom topography does not vary in y-direction, the observed wave motion moving along the alongshore direction at the speed $C'/\sin\theta$ becomes independent in the y-direction. By introducing pseudo-time $\hat{t} = t - (\sin\theta_B / C_B)y$ to unify two independent variable t and y, and assuming the incident wave angle θ_B is small enough to be used as a small parameter, the basic equations are decoupled into independent equations both for longshore motion and cross shore motion.

(b) Particle trajectory in swash zone

Instantaneous behavior of a single spherical particle placed on a uniform slope is simulated under two-dimensional swash motion calculated in the above mentioned model. The momentum equation for the particle is given by

$$
\begin{aligned}
(\rho_s/\rho + C_A)A_3 d^3 \dot{\boldsymbol{u}}_s &= \frac{1}{2} C_D A_2 d^2 |\boldsymbol{u} - \boldsymbol{u}_s|(\boldsymbol{u} - \boldsymbol{u}_s) \\
&\quad + (1 + C_A)A_3 d^3 \dot{\boldsymbol{u}} - (\rho_s/\rho - 1)A_3 g d^3 \sin S \\
&\quad - (\rho_s/\rho - 1)A_3 g d^3 \tan\phi \cos S \cdots\cdots\cdots\cdots (1)
\end{aligned}
$$

in which, g: gravitational acceleration, ρ and ρ_s: specific gravity of water and sediment, d: sediment particle diameter, A_2, A_3: 2- and 3- dimensional shape factor of sediment particle, ϕ : internal friction angel, C_A, C_D: added mass and drag coefficient, u, u_s : fluid and sediment particle velocity vector, respectively.

Since the fluid velocity u has been obtained at every calculation grid, interpolation is needed to calculate u at the point sediment particle locates. The instantaneous position of the particle can be calculated by integrating sediment particle velocity u_s with a time increment of 1/1000 of the wave period.

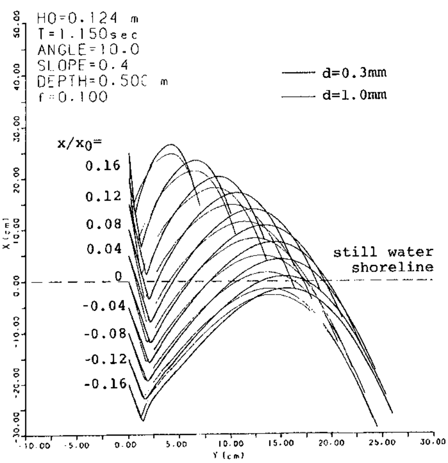

Fig. 1

Trajectories of a sediment particle in a swash zone

Fig. 1 shows one example of the calculated trajectories of a single particle placed on a relatively steep slope S=0.4 to emphasize the gravitational effect. Here, x- and y- axis is chosen to be in the normal and parallel direction to the shoreline, respectively. The results reproduce the zig-zag transport under which a particle is conveyed onshore with a certain angle to the shoreline, then transported offshore with greater angle due to the gravity.

(c) Sediment Transport Rate

Instantaneous sediment transport rate was calculated based on Kobayashi's(1982) bed load formula, which accounts for the effect of a slope explicitly. In the model, the composing forces acting on a spherical particle are the submerged weight, frictional force, fluid drag and lift forces. An inertia force acting on the particle was neglected in the model for simplicity.

To illustrate the external force of a sediment particle, the temporal variations of on-offshore velocity at the still water shoreline x=0 are shown in Fig. 2. The parameter of Fig.2 (a) and (b) is the wave period T and the slope steepness S, respectively. The results show that each velocity fluctuation in swash zone rapidly increases at a passage of bore-like crest, and has long lasting backwash motion. Even though the incident wave height is same in the figures, the breaking wave height H_b will change by the parameter T and S, and that leads to different set-up height at the still water shoreline. The magnitude of the backwash flow is found to be large because the precedent onshore mass flux should be returned through a thin backwash flow. These figures show greater integrated areas in the offshore direction than those in the onshore direction.

The variations of sediment transport rate reflect the velocity variations shown above. Fig. 3(a),(b) illustrates the instantaneous on-offshore transport rates q_x/wd (w: sediment fall velocity) at the still water shoreline x=0. At the limit of horizontal bed, Kobayashi's formula yields that the sediment transport rate is proportional to the Shields number $\Psi(t)$ to the power of 1.5 (3 rd power of the instantaneous fluid velocity). As a result, the curves of sediment transport rate in Fig. 3 show steeper peaks than those in Fig. 2. Fig. 3(b) shows the results with a slope steepness S as a parameter. The steeper the bottom slope, the sharper the onshore transport fluctuations and the greater and the longer the offshore transport fluctuations.

Fig. 4 depicts the instantaneous alongshore transport rate q_y. The alongshore transport is generated mainly during wave up-rush under mild slope condition. Meanwhile, under steep slope condition, a large amount of alongshore transport is observed during down-rush.

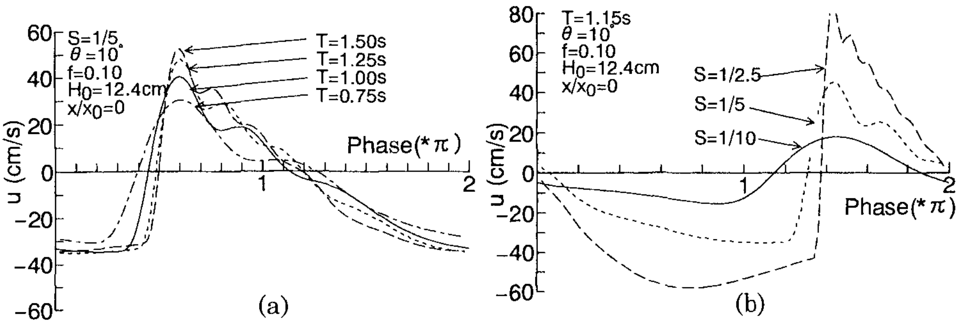

Fig. 2 Temporal variations of on-offshore velocity at x/xo =0

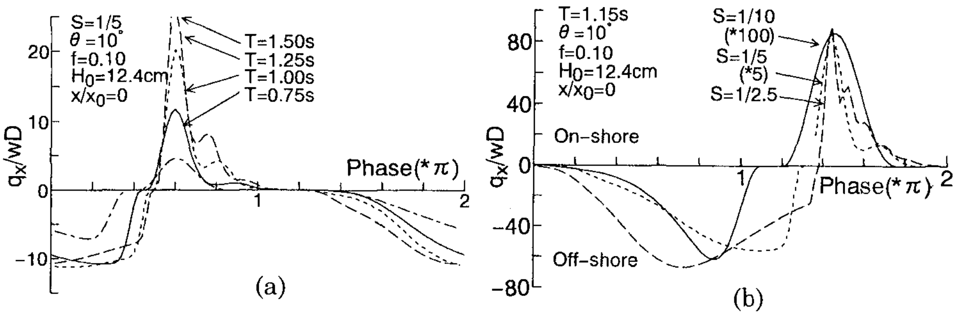

Fig. 3 Temporal variations of on-offshore sediment transport rate at x/xo =0

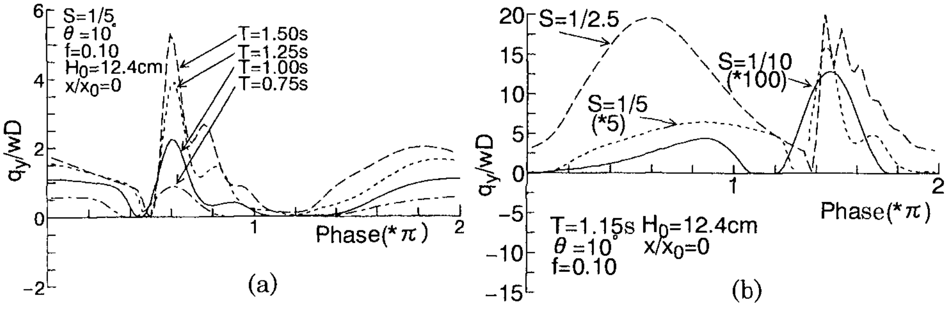

Fig. 4 Temporal variations of alongshore sediment transport rate at x/xo =0

Fig. 5 and Fig. 6 depicts spatial variations of time averaged on-offshore and alongshore sediment transport rates Qx, Qy, respectively. The positive direction of the abscissa is taken in the onshore direction from S.W.S.L.. It is recognized that substantial values both for Qx and Qy are observed even in the onshore region of the shoreline. The time dependent calculation treating the swash wave front as a moving boundary is able to reproduce non-vanishing transport rates both Qx and Qy in the region $x/x_0>0$. These figures show that Qx are offshore direction except for the mildest case $S=1/20$, and Qy decreases monotonously toward the onshore direction, hence, no bi-modal peak around the shoreline is obtained.

(d) Comparison with Conventional Experimental Data

Kamphuis(1990) conducted three-dimensional mobile bed experiments, and investigated alongshore sediment transport rate in swash zone as well as surf zone. Most distributions of his data exhibited bimodal with one peak close to the breaking zone and another in the swash zone. One example of his data is shown in Fig. 7. The ratio of suspended load and bed load throughout his tests showed roughly constant for the entire region, even near the breaking point where suspend load is expected to be predominant.

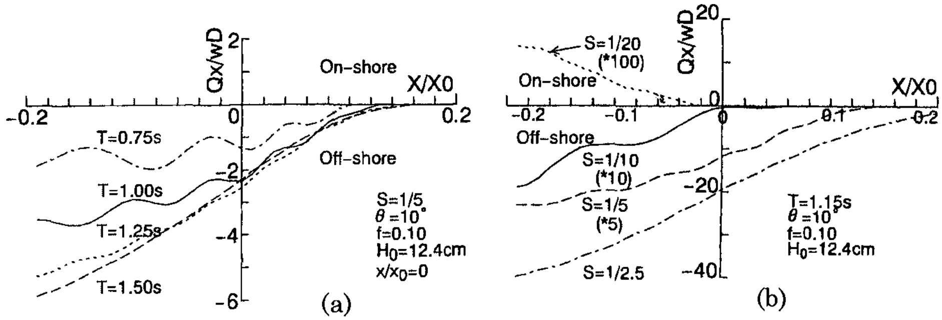

Fig. 5 Spatial variations of time averaged on-offshore sediment transport rate

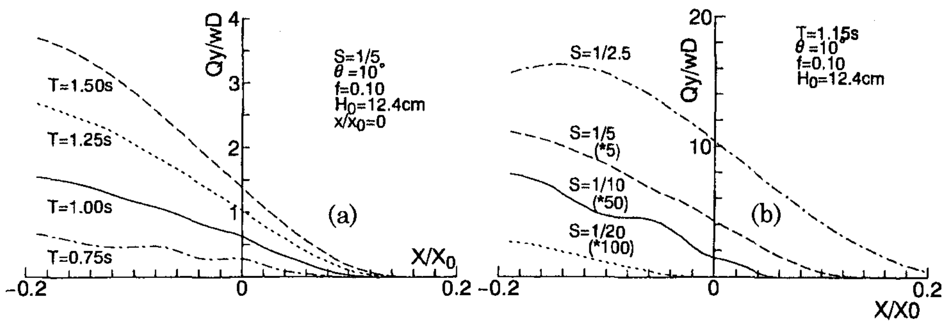

Fig. 6 Spatial variations of time averaged alongshore sediment transport rate

Comparisons with the present calculation under the same input condition of Kamphuis's experiment have revealed that his results were 2 order greater than the calculated results. Fig. 7 shows one of the results where the transport rate Qy at still water shore line x=0 for the bed load was around 17kg/m/hr in its immersed weight. Converting into a non-dimensional transport rate Qy/wd, this amount corresponds to 1.06, while the calculated rate is 0.029.

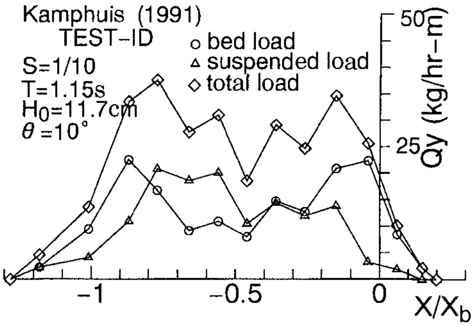

Fig. 7 Distributions of alongshore sediment transport rate (Kamphuis, 1991)

Sunamura(1984) measured on-offshore sediment transport rate focusing on the swash zone in a two-dimensional wave tank. Based on the results, he proposed a transport rate formula for the swash zone. Comparisons between the calculated on-offshore sediment transport rates Qx at x=0 with those of Sunamura's empirical formula are shown in Fig. 8, in which the parameter H_0, T, d is the incident wave height, wave period and sediment diameter, respectively. Qualitative agreements are fairly good in all the figures, but some discrepancies are found. In Fig. 8(a), Sunamura's formula predicts positive Qx values for small wave height, which implies onshore sediment transport corresponding accretional beach formation. Meanwhile the calculated Qx also decreases to zero with decreasing of wave tractive force but the direction is still offshoreward.

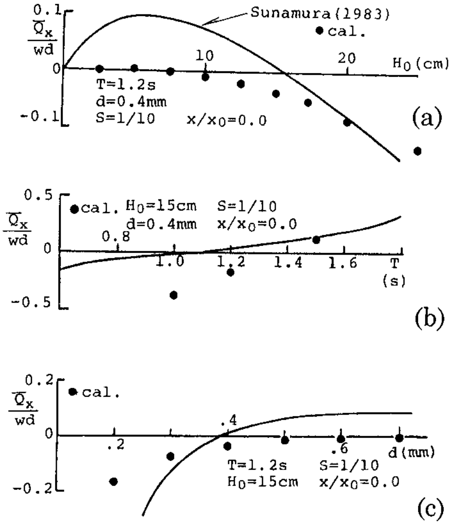

Fig. 8 Comparison of calculated on-offshore sediment transport rate with Sunamura's(1984) formula

The present calculations deal only with bed load transport under non-breaking waves. Large amount of sediment will be suspended by the vortex when the backwash collides with the incoming bore. The discrepancy from the empirical formula suggests the significant contribution of the generated vortex.

3. EXPERIMENTAL STUDY

(a) Experimental Apparatus

The wave tank used here was 26.7m long, 13m wide and 1.2m deep wave basin in Dept. of Ocean Civil Engrg., Kagoshima Univ.(Fig. 8). In this section, the x-axis is taken positive in the offshore direction with the origin x=0 at the still water shoreline. The y-axis is taken in the alongshore direction. A uniform concrete slope of gradient S=1/7.5 was set up at an angle $\theta=15^\circ$ with a wave generator equipped at the other end of the basin. The uniform water depth in the offshore region was kept at constant 79cm throughout the experiments.

Ten capacitance type wave gauges were used, one for the offshore waves, and nine were set in an array on the slope from 210cm offshore to 40cm onshore of the still water shoreline(S.W.S.L.), which covered the surf and swash zone. The wave gauges were inserted into slit holes, which were ditched in order to maintain small water depth even when the bed was dried up at the downrush phase.

A 10mm thick sand layer extending 1.0m width by 3.2m length was laid on the mortar bed. The sand used here was clastic sediment particle originated from igneous rock, of which diameter d was 0.9mm and specific gravity s was 2.96.

(b) Experimental Procedures

Measurements using the florescent sand tracer were conducted at 16 points with 15cm intervals in the range between x=150cm offshore and x=-75cm onshore of S.W.S.L. First, natural undyed sand was laid and leveled its surface accurately. Then, using a core sampler of 36mm inner-diameter and a thin spatula, a cylindrical sand mass was removed. Instead of this, a cylindrical plug of florescent colored sand was buried. After one minute wave action on the sand bed, core samples were collected at 16 points each for two concentric circles of 20cm and 40cm radius.

The samples were evaporated in a drying oven, then, weighed on a precision balance. Meanwhile, the weight

Table-1 Test conditions

	H_i (cm)	T (s)	x_b (cm)	W_u (cm)	ξ
CASE-5	6.4	2.5	-70	85	1.65
CASE-6	7.9	2.0	-60	70	1.19
CASE-7	3.3	3.0	-70	100	2.75
CASE-8	7.5	1.5	-65	65	0.91

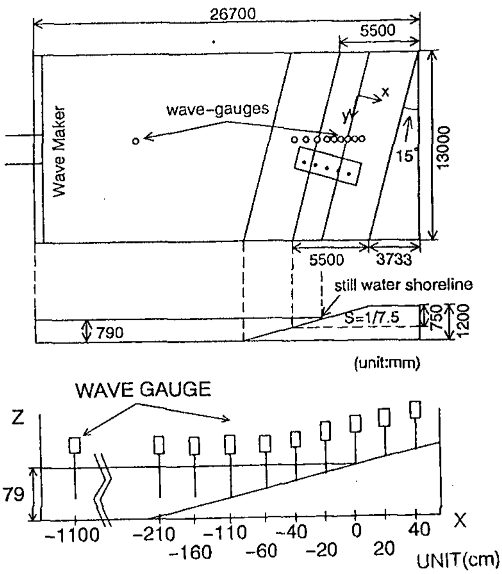

Fig. 8 Wave tank

of dyed sand was estimated by the number which was determined by visual counting under ultraviolet illumination. For this conversion, a calibration curve between the number of particles and its weight was determined beforehand. The final results were arranged in volumetric concentration; the occupation ratio of dyed sand against the whole sand.

Assuming advection is predominant, the sediment transport velocity was estimated in the following way. If a particle initially located at the center moves to the position (r, θ) after Δt time, the traveling velocity for on-offshore and alongshore direction u_s, v_s will be given by r cos $\theta / \Delta t$, r sin $\theta / \Delta t$, respectively. The representative sediment transport velocity was estimated by spatial averaging as follows:

$$u_s = \frac{\iint c(r,\theta)\frac{r\cos\theta}{\Delta t}dS}{\iint c(r,\theta)dS} = \frac{\int_0^\infty\int_0^{2\pi} c(r,\theta)\frac{r\cos\theta}{\Delta t}rd\theta dr}{\int_0^\infty\int_0^{2\pi} c(r,\theta)rd\theta dr}$$

$$v_s = \frac{\iint c(r,\theta)\frac{r\sin\theta}{\Delta t}dS}{\iint c(r,\theta)dS} = \frac{\int_0^\infty\int_0^{2\pi} c(r,\theta)\frac{r\sin\theta}{\Delta t}rd\theta dr}{\int_0^\infty\int_0^{2\pi} c(r,\theta)rd\theta dr} \qquad (2)$$

However, the number of the measuring points was restricted as 16 for each concentric circle, 32 in total, thus the estimation for u_s, v_s was actually carried out by the following equations.

$$u_s = \frac{\sum_{i=1}^{16} c_i \frac{r_1^2\cos\theta}{\Delta t} + \sum_{j=1}^{16} c_j \frac{r_2^2\cos\theta}{\Delta t}}{\left(\sum_{i=1}^{16} c_i\right)r_1 + \left(\sum_{j=1}^{16} c_j\right)r_2}$$

$$v_s = \frac{\sum_{i=1}^{16} c_i \frac{r_1^2\sin\theta}{\Delta t} + \sum_{j=1}^{16} c_j \frac{r_2^2\sin\theta}{\Delta t}}{\left(\sum_{i=1}^{16} c_i\right)r_1 + \left(\sum_{j=1}^{16} c_j\right)r_2} \qquad (3)$$

The test conditions are summarized in Table-1, in which Hi is the incident wave height in uniform depth region, x_b is the location of breaking wave, and W_u is the maximum run-up distance on the slope obtained by eye-measurements.

(c) Wave characteristics on a slope

Fig.9 shows the water surface fluctuations at each measuring point from offshore to onshore. From the fluctuation records, the following parameters were defined to describe the sediment transport; wave height, skewness (asymmetry in respect of horizontal level), asymmetry (asymmetry in respect of center line).

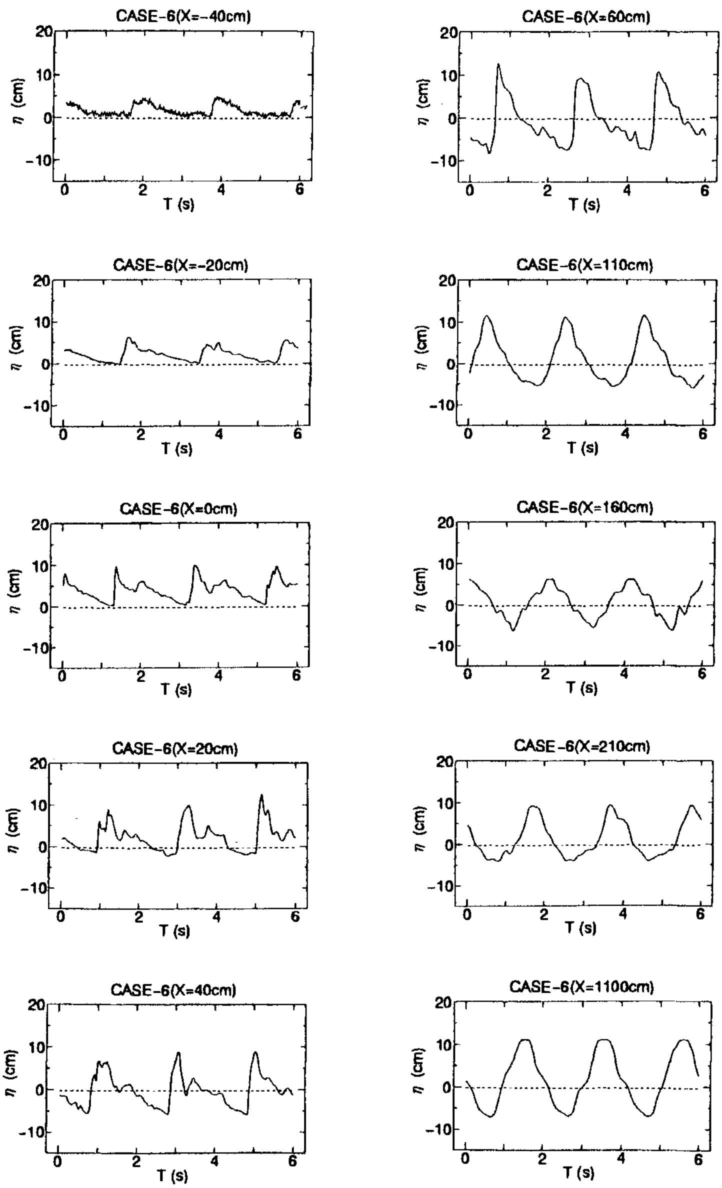

Fig. 9 Measured water surface fluctuations

The definitions of skewness and asymmetry are given by

$$skewness = \frac{1}{\eta_{rms}^{3}} \overline{(\eta - \overline{\eta})^{3}}$$

$$asymmetry = (t_{peak} - t_0)/T$$

in which, η : water surface fluctuation, η_{rms}: root mean square of η、t_0: time at the lowest water surface fluctuation, t_{peak} : time at the succeeding fluctuation peak.

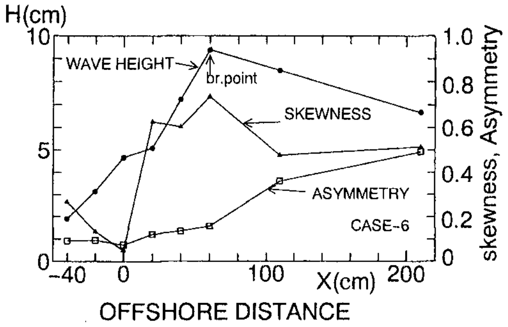

Fig. 10 Spatial variations of wave profile properties

Fig. 10 illustrates that *skewness* becomes small in the swash zone where the water surface fluctuation shows bore-like variation. Meanwhile, *asymmetry* monotonously decreases toward onshore. This sudden increase of wave profile will cause significant onshore-ward sediment transport in the swash region.

(d)Transport velocity determined by tracers

Fig. 11 shows an example of directional distribution of florescent sand concentration. Onshore transport predominance in the offshore region of the breaking point(in this case;x=70cm), alongshore transport in the surf region, and onshore transport around still water shoreline (x=0) are observed. Large scattering was found in the surf zone, where not only advection but diffusion contributes the tracer transport.

The sediment transport velocities estimated from Eq. (3) are plotted in a vector form(Fig. 12). In the figure, the solid vector indicates the data where more than 10 florescent sands were sampled, the dotted vector points out the data where 6 ～ 10 florescent sands were found (less reliable). Following characteristics are obtained:

In the offshore region of the breaking point(B.P.) sediment is transported onshore because the velocity fluctuations are skewed in the onshore direction.

In the region between the breaking point and still water shoreline, alongshore transport is predominant. This is due to generated longshore current in this region. For on-offshore transport, the onward sediment transport due to the skewness of velocity fluctuation may be almost canceled by offshore transport due to an undertow generated near the bottom.

In the swash zone, the transport direction is offshore (except for CASE-7). Since water mass running up on a slope will be returned in a thin layer flow, the velocity of the return flow becomes large enough to transport the sediment offshore in averaging over a period.

The result of CASE-7 is slightly different from others especially in the swash zone , it could be because the wave period was the longest among all the cases, so the breaking type became collapsing (surf similarity parameter in this case ξ =2.75) which breaks suddenly close to the shoreline.

(e) Comparison with the calculated transport velocity

In order to check the validity of the experimental results, calculations based on Kobayashi's formula are performed under the same input condition as the experiments. The results are illustrated in Fig. 13. All of the on-offshore components of transport velocity vector direct offshore. This directional property agrees with the experiment in the swash zone, but disagree in the surf zone and offshore zone.

The comparison also shows the discrepancy in the magnitude of transport velocity. For the experiment, most of the results ranges 0.3 ～ 0.4cm/s, and maximum is 0.66cm/s, which is so small compared to the calculation. In terms of a ratio to the generated longshore current velocity, the data were not so small, but agreed with existing field data. Nadaoka et al.(1981) reported that the sand transport velocity was less than 1.0cm/s, which corresponded to 1 ～ 2 % of the observed longshore velocity.

Several reasons can be considered to explain the difference. One would be due to the large grain size. In this experiment, relatively coarse sand d=0.9mm was used. This might be beyond the applicability of Kobayashi formula which calibrated with existing data using medium and fine sand. The run-up waves propagate on a slope with generating much turbulence at the front. In the numerical model, the velocity field is treated as uniform and no-turbulence, the predictablity of sediment transport in the swash zone is severely restricted.

4. CONCLUSIONS

(1) Analysis on single particle trajectory reproduces the zig-zag sediment movement, which is inherent transport mechanism in the swash zone.

(2) The time dependent analysis treating the swash wave front as a moving boundary enable the calculation to reproduce the swash zone sediment transport. Non-vanishing transport rates both for on-offshore and alongshore directions have been obtained even for the onshore region of the still water shoreline.

(3) From the experiments using florescent sand tracers, the sediment transport in the swash zone is comparable in the magnitude with those in the surf zone, and to be directed generally offshore. The offshore transport can be explained due to the strong backwash flow prevailing over the onshore flow generated at a passage of bore-like front.

(4) The present model postulates uniform velocity distribution and no turbulence. Quantitatively, the model could not reproduce the sediment transport rate in the existing and present experiments. For improving model to describe sediment transport in a swash zone, vortex and turbulence roles for sediment stirring up mechanism should be included.

REFERENCES

Asano, T. H. Suetomi and J. Hoshikura(1994): Measurements of current velocity generated in swash zone by obliquely incident waves, Coastal Engrg., in Japan, Vol. 37, No. 2, pp.125-136.

Asano, T. (1994): Swash motion due to obliquely incident waves, Proc. of 24 th I.C.C.E., ASCE, Vol.1, pp.27-41.

Bodge, K. R. and R. G. Dean(1987): Short-term impoundment of longshore transport, Proc. of Coastal Sediment '87, pp.468-483.

Kamphuis, J.W. (1991): Alongshore sediment transport rate distribution, Proc. of Coastal Sediment'91, pp.170-183.

Kobayashi, N. (1982): Sediment transport on a gentle slope due to waves, J. Waterways, Port, Coastal and Ocean Div., Vol. 108, No. WW3, pp.254-271.

Ryrie, S. C. (1983): Longshore motion generated on beaches by obliquely incident bores, J. Fluid Mech., Vol. 129, pp.193-212.

Sunamura, T. (1984): Onshore-offshore sediment transport rate in the swash zone of a steeply inclined laboratory beach, Ann. Rep., Inst. Geosci., Univ. Tsukuba, No.10, p.69-72.

White, T.E. and D. L. Inman(1989): Measuring alongshore transport with tracers, Nearshore Sediment Transport, Edited by R. J. Seymore, Plenum Press, pp.287-312.

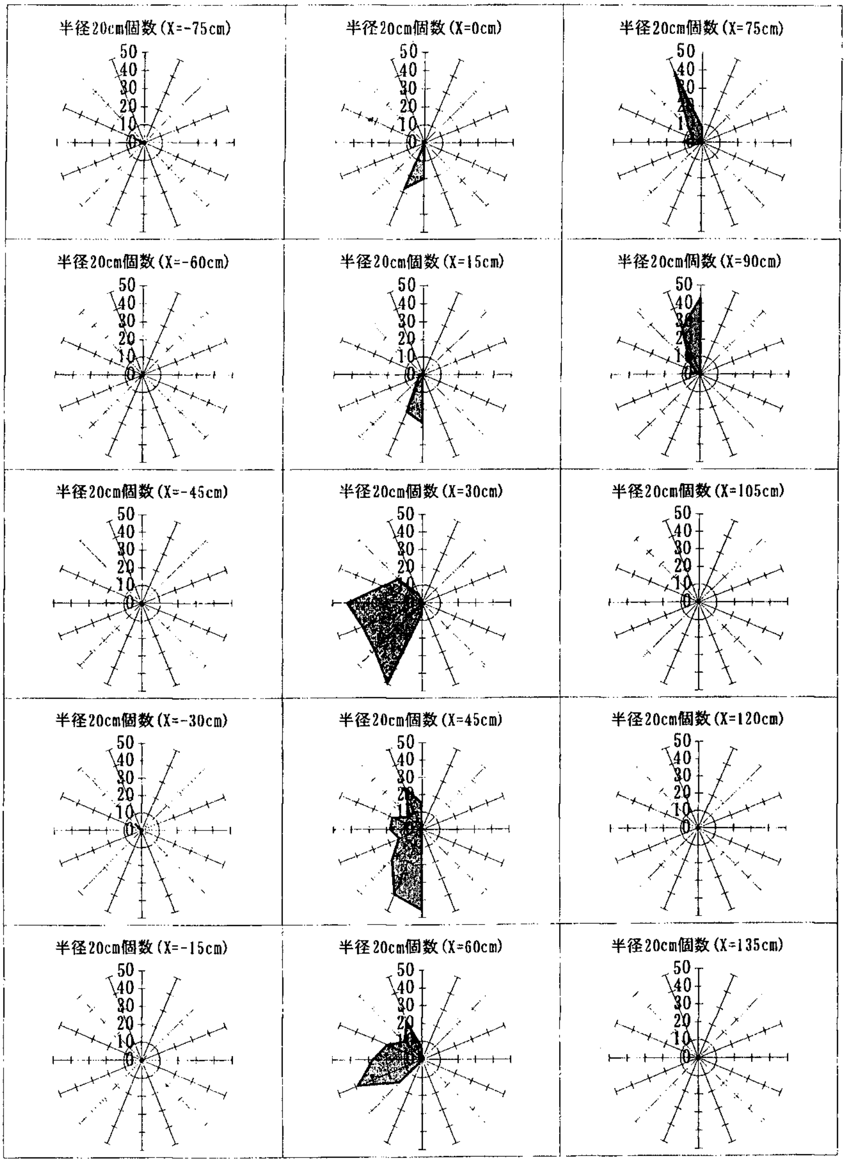

Fig. 11 Directional distributions of florescent sand tracers

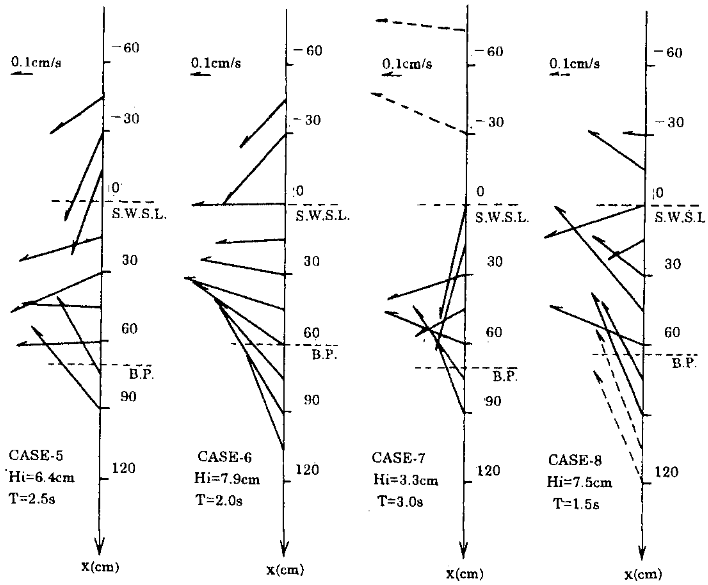

Fig. 12 Measured sediment transport velocity vectors

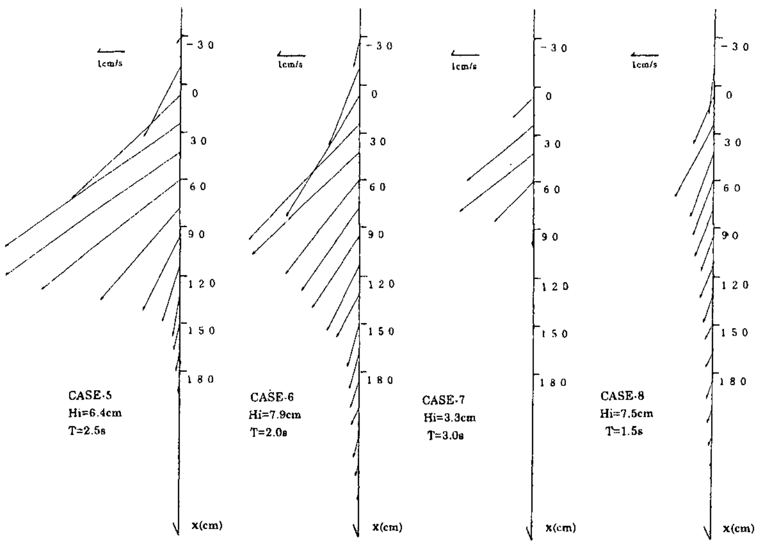

Fig. 13 Calculated sediment transport velocity vectors